Upper critical field in two-band superconductivity

M. Mansor
Department of Physics, Al-Fateh University, Tripoli, Libya

J. P. Carbotte
Department of Physics and Astronomy, McMaster University, Hamilton, Ontario, Canada L8S 4M1
(Received 11 November 2004; revised manuscript received 15 March 2005; published 25 July 2005)

We use a generalization of the Werthamer-Helfand-Hohenberg equations to strong coupling and to two-band superconductivity to study the dependence of the upper critical field $H_{c2}(T)$ on anisotropy in the electron-phonon coupling and in the Fermi velocities, as well as on arbitrary values of intraband and interband impurity scattering. For a layered system such as MgB_2, the temperature dependence of the critical magnetic (H) field itself and the anisotropy ratio $H_{c2}^{ab}(T)/H_{c2}^{c}(T)$ between ab (H in the basal plane) and c (H perpendicular to the basal plane) directions are studied. For MgB_2, the anisotropy ratio is found to be particularly sensitive to intraband impurity scattering in the π band.

DOI: 10.1103/PhysRevB.72.024538 PACS number(s): 74.70.Ad, 74.20.−z, 74.25.Op

I. INTRODUCTION

MgB_2 discovered by Nagamatsu *et al.*[1] has a critical temperature of 39 K and is thought to be an electron-phonon superconductor with the important difference, as compared with conventional cases, that it has two distinct bands with two gap values (each isotropic s-wave). A large superconducting gap exists in a quasi-two-dimensional σ band with a much smaller gap in the three-dimensional π band.[2,3] This is confirmed in electronic band-structure calculations extended to provide a detailed evaluation of the electron-phonon spectral densities.[4–6] Four such quantities are required to describe the superconductivity and particularly its anisotropy: one each for the intraband interaction within the σ and π bands, respectively, and two for the interband contribution. These last two are related by the ratio of the electronic density of states in the π and σ band. A remarkably consistent picture has emerged from such calculations and from comparison with many experimental results on the properties of its superconducting state, most recently being reviewed by Nicol and Carbotte.[7]

A feature of the experimental data on the upper critical field of MgB_2 that is particularly important to understand is the large temperature dependence found in its anisotropy ratio γ_H defined as $\gamma_H(T)=H_{c2}^{ab}(T)/H_{c2}^{c}(T)$, where ab and c refer to the orientation of the magnetic field H in the plane and perpendicular to it.[8–11] Such large anisotropy is not observed in conventional systems and, as stressed recently, cannot be understood in terms of anisotropic Ginsburg-Landau theory.[12,13] An early review was given by Kogan and Bud'ko.[14] The problem was also addressed by Gurevich[15] based on the dirty limit Usadel equations and by Dahm and Schopohl[16] based on the quasiclassical approach of the Eilenberger equations. In this paper, we wish to use a more general approach to the upper critical field valid for arbitrary impurity scattering which is based on the Eliashberg theory. This represents an extension of previous work.[17] The basic equations are a generalization of the original works of Werthamer, Helfand, and Hohenberg (WHH)[18] to include details of the electron-phonon interaction[19] neglected in BCS theory. The paper by Schossmann and Schachinger[20] gives the required generalizations and that of Prohammer and Schachinger[21] treats the multiband case. These equations were used by Shulga *et al.*[22] to treat $H_{c2}(T)$ in the borocarbides. All these works assume an isotropic three-dimensional Fermi surface. A generalization by Prohammer and Carbotte[23] accounts for the possibility of effective-mass anisotropy between the ab and c axes but includes a single band. Here we begin by generalizing this case to include two bands, one which is isotropic and three-dimensional (a model for the π band in MgB_2) and the other ellipsoidal and quasi-two-dimensional (a model for the σ band in MgB_2). Within this model, the necessary equations simplify greatly and we can easily treat any electron-phonon spectral density and arbitrary intraband as well as interband elastic scattering.

Our aim is to understand the influence electron-phonon anisotropy has on the temperature dependence of the critical field with particular attention paid to the effect of the interband components. If these were zero they would give rise to two decoupled superconductors, each with its own critical temperature. It is the interband matrix elements that integrate the subsystems. We are also interested in understanding the role they play in the anisotropy ratio γ_H defined above. Further, we want to treat not just the clean and dirty limit, but also arbitrary values of the intraband and interband impurity scattering rates. Another more minor objective is to study the effect of strong-coupling corrections coming from retardation effects in the electron-phonon spectral densities.

In Sec. II, we present the basic equations from which the upper critical field is calculated. They are a set of two linear equations for the renormalized Matsubara frequencies, which include electron-phonon and impurity contributions, and another two equations for the gaps. The appropriate generalization of the work of Prohammer and Schachinger[21] and Prohammer and Carbotte[23] on which these are based is given briefly in the Appendix. In Sec. III, we describe the effect interband electron-phonon coupling has on the resulting temperature dependence of $H_{c2}(T)$ and on the anisotropy $\gamma_H(T)$. We consider as well interband impurity scattering on $H_{c2}(T)$.

In Sec. IV, we reduce the basic Eliashberg theory through a two-square-well model to a renormalized BCS form (RBCS). This has the advantage that analytical results can be obtained in two important limits. Near T_c we can obtain the slopes and curvature of $H_{c2}(T)$ for any value of intraband impurity scattering, also in the dirty or clean limit for either of the two bands, the zero-temperature value of $H_{c2}(0)$ in special cases. It also allows us, through comparison between numerical results based on the Eliashberg formulation and on RBCS, to identify strong-coupling corrections. In Sec. V, we deal with the anisotropy ratio $\gamma_H(T)$. We employ a model specific to MgB_2 and consider the effect of intraband as well as interband impurity scattering. We derive simple analytic formulas for $H_{c2}(0)$, $h_{c2}(0)$, $\gamma_H(0)$, and $\gamma_H(T_c)$ in the case when there is no gap anisotropy. The formulas are very useful and give insight into the numerical results obtained for the more general case. Another analytic result for the curvature of $H_{c2}(T)$ at T_c clearly shows the role played by Fermi velocity anisotropy in this quantity. We obtain formulas for the effect of anisotropy on the curvature which are particularly simple in the clean limit. Intraband impurity scattering in the σ band is found to rapidly increase the curvature at T_c as well as the value of $h_{c2}(0)$, while for impurities in the π band, the curvature rapidly decreases from its clean limit value to near zero. While $h_{c2}(0)$ also rapidly decreases toward approximately 1.0 as $t^+_{\pi\pi}$ increases, at larger values it begins to show a steady but modest increase. Finally, a summary of our main results is given in Sec. VI, where we present our conclusions.

II. STRONG-COUPLING FORMULATION

As in the previous work of Prohammer and Carbotte[23] for the one-band case, we consider the first band (the σ band) to be quasi-two-dimensional and describe its anisotropy with a simple effective-mass model characterized by the ratio m_σ/M_σ of the *ab* plane mass m_σ to the *c*-direction mass M_σ. In addition, we consider the second band (the π band) to be three-dimensional and isotropic with mass m_π. In their previous work, Prohammer and Schachinger[21] considered the multiband[24] case but without effective-mass anisotropy. Some relevant details of our generalization are found in the Appendix.

The equations for the upper critical magnetic field $H_{c2}(T)$ are[19]

$$\tilde{\omega}_i(n) = \omega_n + \pi T \sum_{m,j} [\lambda_{ij}(m-n) + \delta_{m,n} t^+_{ij}/T] \mathrm{sgn}[\tilde{\omega}_j(m)]. \tag{1}$$

$$\tilde{\Delta}_i(n) = \pi T \sum_{m,j} \{[\lambda_{ij}(m-n) - \mu^\star_{ij}] + \delta_{m,n} t^+_{ij}/T\} \chi_j(m) \tilde{\Delta}_j(m), \tag{2}$$

with

$$\chi_i(n) \equiv \chi_i[\tilde{\omega}_i(n)] = \frac{2}{\sqrt{\alpha_i \kappa_i}} \int_0^\infty dq e^{-q^2} \tan^{-1}\left(\frac{q\sqrt{\alpha_i \kappa_i}}{|\tilde{\omega}_i(n)|} \right), \tag{3}$$

with

$$\alpha_i = \frac{e}{2} H_{c2}(T) v^2_{Fi}. \tag{4}$$

In these equations, $\omega_n = \pi T(2n-1)$, $n = 0, \pm 1, \pm 2, \ldots$, are the unrenormalized Matsubara frequencies with T the temperature. In Eq. (1), $\tilde{\omega}_i(n)$ is the renormalized Matsubara frequency due to the interaction of electrons with the phonons described by λ_{ij} and the impurities t^+_{ij}. In terms of the electron-phonon spectral density $\alpha^2_{ij}F(\omega)$, we have

$$\lambda_{ij}(n-m) = \int \frac{2\Omega \alpha^2_{ij} F(\Omega) d\Omega}{\Omega^2 + (\omega_n - \omega_m)^2}, \tag{5}$$

and the impurity parameters $\pi t^+_{ij} = 1/2\tau_{ij}$, where τ_{ij} are impurity scattering times. In Eq. (2), $\tilde{\Delta}_i(n)$ is the gap and $\mu^\star_{ij}$ is the Coulomb pseudopotential. The label $i = 1, 2$ for the σ and π band, respectively. In Eq. (3), κ_i is the band anisotropic effective-mass parameter introduced by Prohammer and Carbotte,[23] and here it is different from unity only for the σ band, in which case it has the form

$$\kappa_\sigma(\theta) = \sqrt{\cos^2(\theta) + \mu \sin^2(\theta)}, \tag{6}$$

where θ is the direction of the external magnetic field with respect to the *c* axis and $\mu = m_\sigma/M_\sigma$. Equations (3) and (6) give the angular dependence of $H_{c2}(T)$ with θ. Finally, in Eq. (4), e is the charge on the electron and v_{Fi} is the Fermi velocity of each band. When the effective-mass anisotropy in Eq. (6) is not included, our equations reduce to the two-band model of Prohammer and Schachinger.[21] In weak coupling they reduce to the usual multiband version[24] of the well known equations of WHH.[18] When only the σ band is considered, they reduce to those of Prohammer and Carbotte.[23] Equations (1) and (2) apply for any value of the impurity parameters t^+_{ij} and so include the dirty and clean limits. Note that we also take fully into account interband scattering.

III. ROLE OF OFF-DIAGONAL INTERACTIONS

The electronic band structure of MgB_2 is well understood and consists of four bands nearly degenerate in pairs. In the past the quasi-two-dimensional σ band was modeled by a distorted cylinder,[16] and the more nearly three-dimensional and isotropic π band was modeled by a half-torus. In this paper, we do not deal explicitly with the full complications of such topological structures but instead model the σ band with an ellipsoidal structure with two effective masses m_σ, M_σ and the π band is taken to be isotropic. Thus we do not try to deal with the explicit case of MgB_2 in all of its details. In keeping with this spirit, it will be sufficient here to use a model for the electron-phonon spectral functions $\alpha^2_{ij}F(\omega)$. These are known from extensive band-structure calculations of the electron-phonon matrix elements.[4–6,25] Here we use instead the $\alpha^2F(\omega)$ known from tunneling inversion for Pb (Ref. 19) stretched, however, to 60 meV with choices of mass renormalization $\lambda_{ij} = 2\int[\alpha^2_{ij}F(\omega)/\omega]d\omega$ for (i,j) close to those for MgB_2. Details of the $\alpha^2F(\omega)$ spectrum are not critical to our results. For a discussion of the effects of Fermi surface topology on the critical field of MgB_2 as well

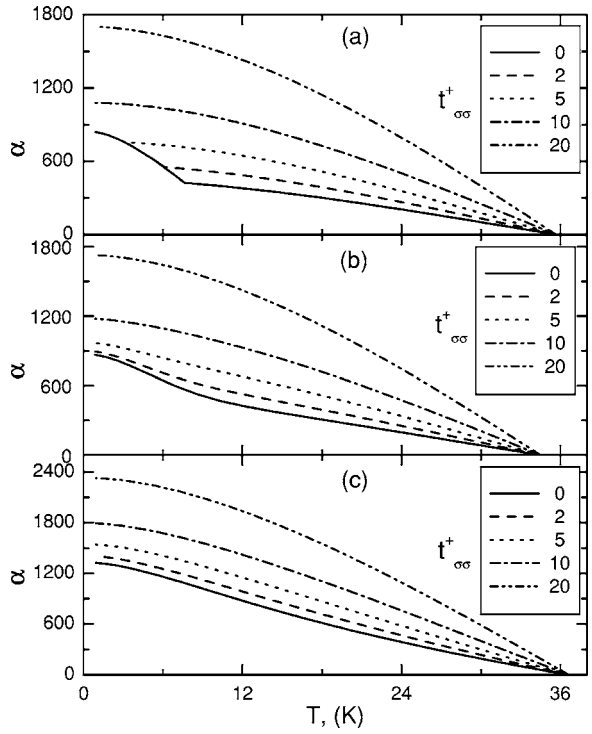

FIG. 1. Upper critical field $H_{c2}(T)$ in arbitrary units ($\alpha = ev_F^2 H_{c2}/2$) as a function of temperature T for a dirty π band with $t^+_{\pi\pi}=60$ meV. The other parameters are $\lambda_{\sigma\sigma}=1.0$ and $\lambda_{\pi\pi}=0.5$. The various curves are as labeled for $t^+_{\sigma\sigma}=0$, 2, 5, 10, and 20 meV. No interband impurity scattering is included. Frame (a) is for $\lambda_{\sigma\pi}=\lambda_{\pi\sigma}=0$ (decoupled bands), frame (b) is for $\lambda_{\sigma\pi}=\lambda_{\pi\sigma}=0.05$, and frame (c) is for $\lambda_{\sigma\pi}=\lambda_{\pi\sigma}=0.2$.

as the effect of other specific aspects of its calculated electronic structure, the reader is refered to Ref. 16.

In Fig. 1, we show results for $H_{c2}(T)$ in arbitrary units as a function of temperature T with $\lambda_{\sigma\sigma}=1$ and $\lambda_{\pi\pi}=0.5$. In frame (a) we have taken $\lambda_{\sigma\pi}=\lambda_{\pi\sigma}=0$, i.e., no coupling between the bands. In this case, the critical temperature for the combined system is that of the σ band. To illustrate an important point, we have taken the σ band (dominant) to have $t^+_{\sigma\sigma}=0$, 2, 5, 10, and 20 meV for bottom to top curves, respectively. In all cases, the π band has a fixed value of $t^+_{\pi\pi}=60$ meV (dirty limit) and the σ band is, therefore, always cleaner. The interband impurity scattering is not considered, i.e., $t^+_{\sigma\pi}=t^+_{\pi\sigma}=0$. For small values of $t^+_{\sigma\sigma}$, the curves for $H_{c2}(T)$ show a crossover at low temperature which corresponds to a switchover from the $H_{c2}(T)$ due to the σ band alone to that of the π band alone. Recall that these bands are completely decoupled. While the π band is the weakest of the two bands, it can nevertheless have, on its own, a larger H_{c2} than the σ band (below its own critical temperature) when it is much dirtier than the σ band. However, as the impurity scattering in the σ band is increased, its critical field also increases, and at some relatively modest value of $t^+_{\sigma\sigma}$, as compared with $t^+_{\pi\pi}=60$ meV, the crossover can no longer occur. We see from Fig. 1 that this takes place between $t^+_{\sigma\sigma}=5$ and 10 meV.

It is instructive to make a simple estimate of the minimum value of $t^+_{\pi\pi}$ which is necessary to get a crossover at some low temperature for the case when the σ band is clean. For a clean band with critical temperature $T_c=T_c^\sigma$ (i.e., that of the σ band alone), the zero-temperature critical field is given by

$$H_{c2}(0)=\left(\frac{\pi}{2}\right)^2\frac{2T_c^{\sigma 2}}{ev_{F\sigma}^2}(1+\lambda_{\sigma\sigma})^2 e^{-\gamma+2}. \tag{7}$$

On the other hand, for the dirty π band,

$$H_{c2}(0)=\frac{3\pi^2 T_c^{\pi}(1+\lambda_{\pi\pi})}{e^{\gamma}v_{F\pi}^2(e)}t^+_{\pi\pi}, \tag{8}$$

where the e multiplying the v_F^2 is the charge on the electron and γ is Euler's constant. In addition, T_c^π is the critical temperature of the π band on its own which is determined by $\lambda_{\pi\pi}$. These equations, are taken from a RBCS reduction of the full Eliashberg equations, as we will describe later. For the moment, except for $\lambda_{\sigma\sigma}$ and $\lambda_{\pi\pi}$ renormalizations, they are the ordinary BCS results of WHH. The criterion for a crossover from the dominant band to the secondary band behavior above $T=0$ is $H_{c2}^\pi(0)>H_{c2}^\sigma(0)$ or $t^+_{\pi\pi}\gtrsim 18T_c$ for the parameters considered here assuming $v_{F\sigma}=v_{F\pi}$, which is a good approximation for the magnetic field H parallel to the c axis in MgB_2. For H in the ab plane, $v_{F\sigma}$ is expected to be much smaller than $v_{F\pi}$. Assuming a factor of 10 for illustration, this gives $t^+_{\pi\pi}\gtrsim 180T_c$ for a crossover to occur in this case. Note that in this second case, our model would predict a crossover from an elliptical pattern to a circular one for the spatial dependence of the gap in the Abrikosov lattice as we pass from the σ to the π band for H parallel to ab.

Frames (b) and (c) of Fig. 1 show how this picture becomes modified when coupling between the bands is included. Frame (b) applies to $\lambda_{\sigma\pi}=\lambda_{\pi\sigma}=0.05$ and frame (c) to $\lambda_{\sigma\pi}=\lambda_{\pi\sigma}=0.2$, otherwise the other parameters are kept the same. Focusing on the lower curve in each frame (i.e, $t^+_{\sigma\sigma}=0$), we note that a finite value of interband electron-phonon coupling leads to a rapid smearing of the crossover region as the bands become integrated. This is true even for $\lambda_{\sigma\pi}=\lambda_{\pi\sigma}=0.05$, although the composite curve in this instance is still recognizable as the superposition of two separate typical single-band $H_{c2}(T)$ curves. As $t^+_{\sigma\sigma}$ is increased, the curves move progressively from two bands (with smearing) to a more conventional single-band H_{c2} pattern. In the region between these two limiting cases, the curves for $H_{c2}(T)$ naturally acquire a quasilinear in T behavior over a large temperature range, although they always turn over at sufficiently low temperatures. We note that as $\lambda_{\pi\sigma}=\lambda_{\sigma\pi}$ is changed, there is also a change in the critical temperature. As previously noted, particularly by Mitrovic[26] and by Nicol and Carbotte,[7] in the Eliashberg theory this change in T_c can be negative for small values of $\lambda_{\pi\sigma},\lambda_{\sigma\pi}$ in contrast to BCS theory, where an increase is always predicted.

In the conventional theory of $H_{c2}(T)$ applicable to a single band, the ratio of the slope of H_{c2} at T_c to its value at $T=0$ plays an important role. In BCS theory, $h_{c2}(0)=|H_{c2}(0)/[T_c dH_{c2}/dT|_{T_c}]|=0.69$ in the dirty limit and 0.727 in the clean limit. Thus, while the slope and $H_{c2}(0)$ depend very much on impurity content, the normalized ratio does not. This can no longer be expected in the two-band case, as

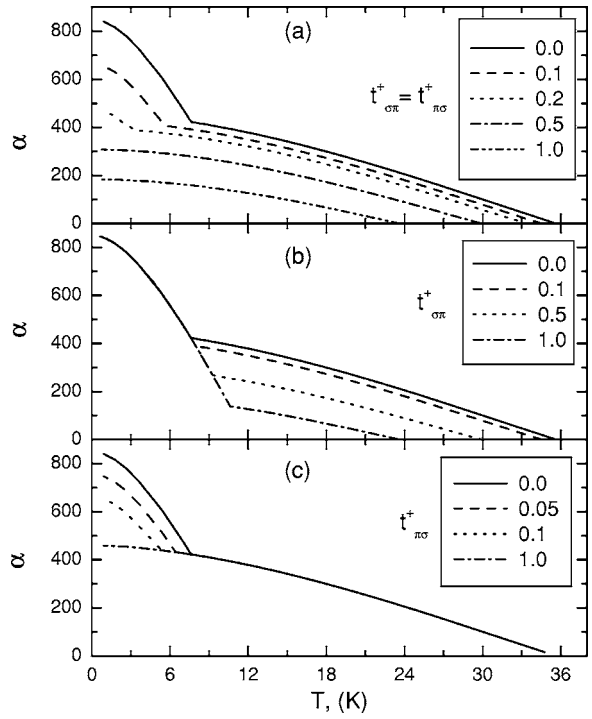

FIG. 2. Upper critical field $H_{c2}(T)$ in arbitrary units ($\alpha = ev_F^2 H_{c2}/2$) as a function of temperature. The parameters are $\lambda_{\sigma\sigma}=1.0$, $\lambda_{\sigma\pi}=0.5$, and $\lambda_{\sigma\pi}=\lambda_{\pi\sigma}=0$. The σ band has $t^+_{\sigma\sigma=0}$ (clean case) while the π band has $t^+_{\pi\pi}=60$ meV (dirty case). In addition, $t^+_{\pi\sigma}=t^+_{\sigma\pi}=0.0$, 0.1, 0.2, 0.5, and 1.0 as labeled in frame (a); $t^+_{\pi\sigma}=0$ and $t^+_{\sigma\pi}=0.0$, 0.1, 0.5, and 1.0 in frame (b); $t^+_{\pi\sigma}=0.0$, 0.05, 0.1, and 1.0 and $t^+_{\sigma\pi}=0$ in frame (c).

can be illustrated simply in the decoupled case $\lambda_{\pi\sigma}=\lambda_{\sigma\pi}=0$ under the assumption that a crossover occurs. In this case the σ band, assumed clean for simplicity, will determine the slope at T_c and the π band, assumed dirty, will determine $H_{c2}(0)$. The normalized $h_{c2}(0)$ for the composite system will take the form

$$h_{c2}(0) = \frac{7\zeta(3)}{24e^{\gamma}}\left(\frac{v_{F\sigma}}{v_{F\pi}}\right)^2 \frac{(1+\lambda_{\pi\pi})}{(1+\lambda_{\sigma\pi})^2}\frac{T_c^{\pi}}{T_c^2} t^+_{\pi\pi}, \tag{9}$$

with the condition that $t^+_{\pi\pi} \gtrsim 18T_c$ for the parameters considered here. In this formula, $\zeta(3)$ is the Riemann zeta function. We find for the parameters of Fig. 1

$$h_{c2}(0) \cong 0.027\frac{t^+_{\pi\pi}}{T_c}, \tag{10}$$

which increases with increasing $t^+_{\pi\pi}/T_c(>18)$ and is greater than the one-band result in the range of validity of Eq. (10).

Next we consider the effect of off-diagonal impurity scattering on the $H_{c2}(T)$ curves in the case where the bands are decoupled, i.e., $\lambda_{\pi\sigma}=\lambda_{\sigma\pi}=0$, and that we are in the regime where a crossover occurs between the σ and π band. In Fig. 2, which has three frames, we show results for the case $\lambda_{\sigma\sigma}=1$, $\lambda_{\pi\pi}=0.5$, and $t^+_{\pi\pi}=60$ meV and $t^+_{\sigma\sigma}=0$ (clean) as in the lowest curve in frame (a) of Fig. 1. In frame (a) of Fig. 2, we have $t^+_{\sigma\pi}=t^+_{\pi\sigma}=0$, 0.1, 0.2, 0.5, and 1.0 meV for the curves ordered from top to bottom. Interband impurity scattering does not smear the crossover point but rather progressively decreases the direct contribution of both the σ and π band with the crossover temperature also dropping toward zero. The direct π-band contribution has disappeared completely at $T=0$ for the case $t^+_{\sigma\pi}=t^+_{\pi\sigma}=0.5$ meV. At the same time, we note that the critical temperature is lowered with increasing interband impurity coupling. While the interband electron-phonon interaction $\lambda_{\pi\sigma}=\lambda_{\sigma\pi}$ is taken to be zero for these curves, it does not mean that the two bands themselves are decoupled when the interband impurity scattering is finite. It is of interest to understand the difference in the role played by $t^+_{\sigma\pi}$ and $t^+_{\pi\sigma}$. The first gives the effect of the π band on the σ band and is, of the two variables, the most effective at changing the value of T_c. This is seen in frames (b) and (c) of Fig. 2 for $t^+_{\sigma\pi}$ and $t^+_{\pi\sigma}$, respectively, with the other set equal to zero. In frame (b), $t^+_{\sigma\pi}$ ranges from 0 to 0.1, 0.5, and 1.0 meV from the top to the bottom curve and in frame (c), $t^+_{\pi\sigma}$ ranges from 0 to 0.05, 0.1, and 1.0 meV. In the last case, T_c is not affected but the direct contribution from the π band is gradually reduced to zero while at the same time the crossover moves toward $T=0$. By contrast, in frame (b) the T_c value is strongly reduced, as is the contribution from the σ band, while that of the π band is not changed. Clearly the effects of $t^+_{\pi\sigma}$ and $t^+_{\sigma\pi}$ are very different. Here, our line of argument is structured as in the previous paper of Nicol and Carbotte,[7] who discuss the specific heat, the thermodynamic critical field, the penetration depth, the energy gap, and other quantities. In this paper, we examine H_{c2} in a similar manner.

The value of the off-diagonal electron-phonon interaction parameter can affect the temperature dependence of the resultant $H_{c2}(T)$ in a different way depending on the other parameters involved, such as, for example, the Fermi velocities of the two bands. This is illustrated in Fig. 3, where we compare a case where both bands have the same Fermi velocity to that when the σ band is different from that for the π band by a factor of $\sqrt{R}$, with $R=\kappa_{\sigma}$. The figure has three frames. In all cases the clean limit is considered, i.e., no intraband or interband impurity scattering. Also $\lambda_{\sigma\sigma}=1.0$ and $\lambda_{\pi\pi}=0.5$. The solid curves are those for equal Fermi velocities while the others are for $R \neq 1.0$. In all cases the curves are normalized to a value of 1 at $T=0$. In frames (a) and (b), the dashed curve is for $R=0.1$ but differ in that $\lambda_{\pi\sigma}=\lambda_{\sigma\pi}=0.2$ [frame (a)] and 0.4 [frame (b)]. Note the upward curvature around T_c in the dashed curves, which becomes more pronounced as the off-diagonal λ's increase. It also becomes more pronounced as R is made to deviate more from unity. This is seen in frame (c), for which $\lambda_{\pi\sigma}=\lambda_{\sigma\pi}=0.2$, but $R=0.01$ for the dashed curve and 100 for the dotted curve. The two cases $v_{F\sigma} \ll v_{F\pi}$ and $v_{F\sigma} \gg v_{F\pi}$ are completely different, with the second changing the temperature dependence of $H_{c2}(T)$ as compared with the solid curve over a much larger range of temperature below T_c. In fact, it is only at T near zero that we now get a match. More insight into the role played by Fermi velocity anisotropy on the curvature of $H_{c2}(T)$ at T_c will be provided in Sec. V after we have considered the reduction of our Eliashberg equations to RBCS, for which case analytic results are possible. This curvature has been widely noted and discussed in both the theoretical[13–16,18,22,27,28] and the experimental[9–12,29–33] literature.

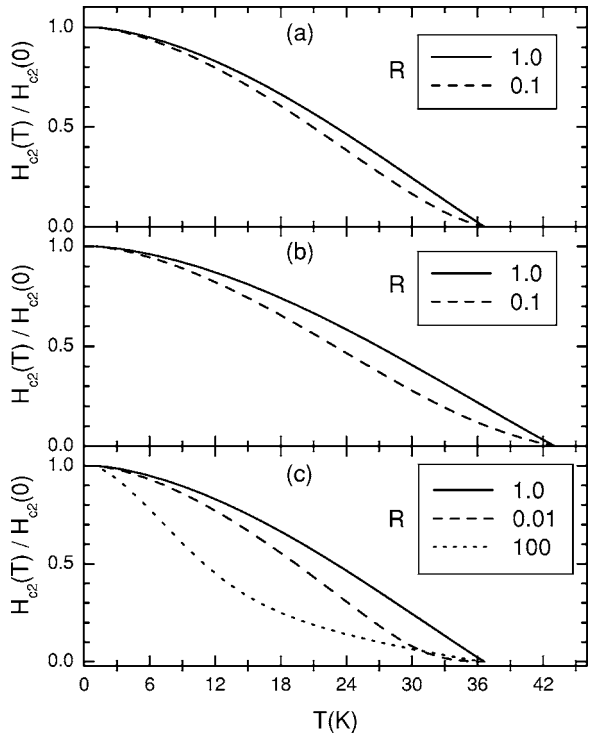

FIG. 3. Normalized upper critical field as a function of temperature. The solid curve is $H_{c2}^{c}(T)$ while the dashed is for $H_{c2}^{ab}(T)$ both normalized to a value of unity at $T=0$. Frame (a) corresponds to $\lambda_{\sigma\pi}=\lambda_{\pi\sigma}=0.2$, frame (b) corresponds to $\lambda_{\sigma\pi}=\lambda_{\pi\sigma}=0.4$, and both have $R=0.1$ for the dashed curve. Frame (c) is for $\lambda_{\sigma\pi}=\lambda_{\pi\sigma}=0.2$, but now $R=0.01$ (dashed) and $R=100.0$ (dotted).

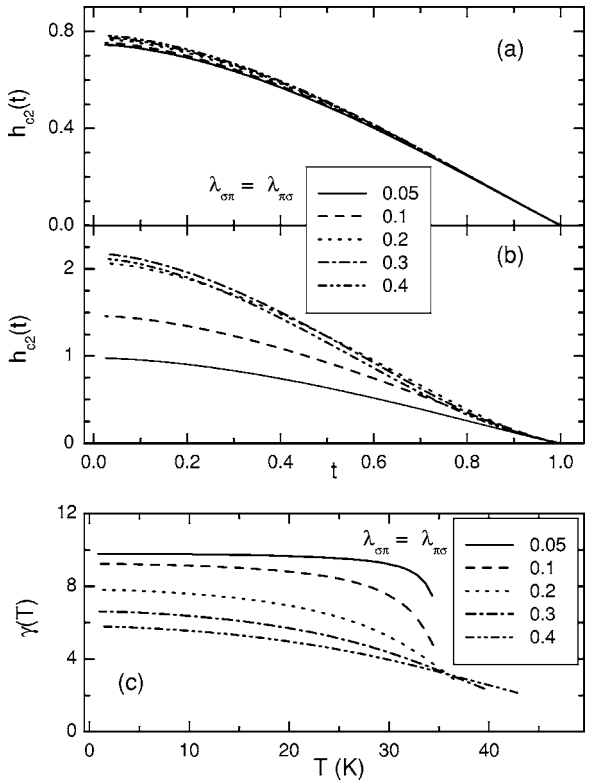

FIG. 4. The critical magnetic field anisotropy parameter $\gamma(T)$ as a function of temperature [frame (c)]. From top to bottom, the curves are for $\lambda_{\sigma\pi}=\lambda_{\pi\sigma}=0.05$, 0.1, 0.2, 0.3, and 0.4 with $t^{+}_{\sigma\sigma}=t^{+}_{\pi\pi}=t^{+}_{\pi\sigma}=t^{+}_{\sigma\pi}=0$ and $R=0.1$. Frame (a) gives $h_{c2}(t)$ for the c direction and frame (b) is for the a-b plane.

An important quantity experimentally is the upper critical field anisotropy ratio $\gamma_H(T)$ defined earlier. In Fig. 4 [frame (c)], we show $\gamma_H(T)$ as a function of temperature for the clean limit ($t^{+}_{\sigma\sigma}=t^{+}_{\pi\pi}=t^{+}_{\sigma\pi}=t^{+}_{\pi\sigma}=0$); here $\lambda_{\sigma\sigma}=1.0$, $\lambda_{\pi\pi}=0.5$, and $\lambda_{\sigma\pi}=\lambda_{\pi\sigma}$ is varied with $R=0.1$. From bottom to top, curves are shown for $\lambda_{\sigma\pi}=\lambda_{\pi\sigma}=0.4$, 0.3, 0.2, 0.1, and 0.05. There is a slight initial decrease in the value of T_c as the off-diagonal λ's increase before it increases. In all cases, increasing $\lambda_{\sigma\pi}=\lambda_{\pi\sigma}$ decreases $\gamma_H(T)$ at zero temperature. The decoupled band limit of $\lambda_{\sigma\pi}=\lambda_{\pi\sigma}=0$ corresponds to $\gamma_H(T)=1/R=10$. Also in the lower curve of Fig. 4 [frame (c)] the temperature variation has been reduced over that for the second lowest ($\lambda_{\sigma\pi}=\lambda_{\pi\sigma}=0.3$). In addition, as $\lambda_{\sigma\pi}=\lambda_{\pi\sigma}$ is increased, the temperature region over which the variation in $\gamma_H(T)$ occurs extends to lower temperature and is no longer mainly confined to the region near T_c as in the top curve. Still, for parameters in the range of those for MgB_2, the anisotropy remains quite significant (dashed and dotted curves). Because our model for the Fermi surface is simpler than that used in Ref. 16 and we include strong-coupling corrections and realistic electron-phonon spectral densities, a direct quantitative comparison is not possible. However, the two sets of results agree in all qualitative aspects. We show in Fig. 4, frame (a) (c direction) and frame (b) (ab plane), the normalized critical field $h_{c2}(t)$ as a function of the reduced temperature t for the same parameters as were used in frame (c). For the magnetic field oriented in the c direction ($R=1$), h_{c2} at $t=0$ remains very near its one-band value, while for the ab direction ($R=0.1$) it is very different and ranges from ~ 1 to $\gtrsim 2$ as the value of the off-diagonal $\lambda_{\sigma\pi}=\lambda_{\pi\sigma}$ is varied. Note that the curve for $\lambda_{\sigma\pi}=\lambda_{\pi\sigma}=0.4$ has a smaller value of $h_{c2}(0)$ than does the one for 0.3. We conclude that the gap anisotropy which results from differences in the electron-phonon parameters λ_{ij} has little effect on $h_{c2}(t)$ when there is no Fermi velocity anisotropy but that it has a large effect when it is accompanied by a large difference between $v_{F\sigma}$ and $v_{F\pi}$ ($v_{F\sigma}<v_{F\pi}$). Finally we note that the upward curvature, seen near T_c in frame (b), is absent in frame (a). This is a second characteristic of Fermi velocity anisotropy.

IV. REDUCTION IN THE $\lambda^{\theta\theta}$ MODEL AND STRONG COUPLING

Ignoring retardation effects in our Eqs. (1) and (2) leads to a great simplification of the equations and allows us to make the connection between Eliashberg results and RBCS. In this model, $\lambda(m-n)$ is assumed to be a constant independent of index m and n and is cut off at some energy ω_c for both ω_m and ω_n in the gap channel. This approximation is often referred to in the literature as the $\lambda^{\theta\theta}$ model. Applying it to Eq. (2) assuming for simplicity that $t^{+}_{\sigma\pi}=t^{+}_{\pi\sigma}=0$ (it can easily be generalized to include finite interband impurity scattering) and replacing Eq. (1) by

$$\tilde{\omega}_i(n) = \omega_n(1 + \lambda_{ii} + \lambda_{ij}) + \pi(t_{ii}^+), \tag{11}$$

and after introducing a new gap,

$$\bar{\tilde{\Delta}}_i(n) = \tilde{\Delta}_i(n)[1 - \pi t_{ii}^+ \chi_i(n)], \tag{12}$$

we obtain

$$\bar{\tilde{\Delta}}_i(n) = \sum_j (\lambda_{ij} - \mu_{ij}^\star)\pi T \sum_m^{\omega_c} \frac{\bar{\tilde{\Delta}}_j(m)}{\chi_j^{-1}(m) - \pi t_{jj}^+}. \tag{13}$$

These are just the generalization of the original WHH equations to two bands with a single change, namely, quantities become renormalized by the electron-phonon mass enhancement parameter of Eq. (11).

A great virtue of Eq. (13) is that analytic results can be obtained at T near T_c and at any temperature when both bands are in the dirty limit. In both cases, the inverse tangent in Eq. (3) can be expanded because its argument is small either because α_i is small (near T_c) or because $\tilde{\omega}_i(n)$ is large and equal to πt_{ii}^+ in the dirty limit. Under such circumstances, we obtain

$$\chi^{-1}[\tilde{\omega}_i(n)] - \pi t_{ii}^+ \cong |\tilde{\omega}_i^0(n)| + \frac{1}{3}\frac{\alpha_i}{|\tilde{\omega}_i(n)|}, \tag{14}$$

where $\tilde{\omega}_i^0(n)$ stands for $\tilde{\omega}_i(n)$ without impurity contribution. Equation (13) becomes

$$\bar{\tilde{\Delta}}_i = \sum_j \frac{\lambda_{ij} - \mu_{ij}^\star}{1 + \lambda_{jj} + \lambda_{ji}} F_j \bar{\tilde{\Delta}}_j, \tag{15}$$

where we have recognized the fact that $\bar{\tilde{\Delta}}_i$ is now a constant independent of n and

$$F_j = \pi T \sum_m^{\omega_c} \frac{1}{|\omega_m| + \frac{1}{3}\frac{\tilde{\alpha}_j}{|\tilde{\omega}_j(m)|}}, \tag{16}$$

with $\tilde{\alpha}_i = \alpha_i/(1+\lambda_{ii}+\lambda_{ij})$, and we also write $\tilde{\lambda}_{ij} = (\lambda_{ij} - \mu_{ij}^\star)/(1+\lambda_{jj}+\lambda_{ji})$. The eigenvalue equation associated with Eq. (15) is

$$1 = \tilde{\lambda}_{\pi\pi}F_\pi + \tilde{\lambda}_{\sigma\sigma}F_\sigma + (\tilde{\lambda}_{\pi\sigma}\tilde{\lambda}_{\sigma\pi} - \tilde{\lambda}_{\pi\pi}\tilde{\lambda}_{\sigma\sigma})F_\pi F_\sigma. \tag{17}$$

Solving Eq. (17) for the highest eigenvalue gives $H_{c2}(T)$ near T_c. After lengthy but straightforward algebra, one finds

$$H_{c2}(T) = \frac{(1-t)\frac{12}{e}A(\pi T_c)^2}{[(\tilde{\lambda}_{\sigma\sigma} - \tilde{\lambda}_{\pi\pi}) + A]\tilde{v}_{F\sigma}^2 g_\sigma + [(\tilde{\lambda}_{\pi\pi} - \tilde{\lambda}_{\sigma\sigma}) + A]\tilde{v}_{F\pi}^2 g_\pi}, \tag{18}$$

where

$$A = \sqrt{(\tilde{\lambda}_{\sigma\sigma} - \tilde{\lambda}_{\pi\pi})^2 + 4\tilde{\lambda}_{\sigma\pi}\tilde{\lambda}_{\pi\sigma}}, \tag{19}$$

and

$$g_i = g\left(\frac{\tilde{t}_{ii}^+}{T_c}\right),$$

$$\tilde{t}_{ii}^+ = t_{ii}^+/[1 + \lambda_{ii} + \lambda_{ij}],$$

$$\tilde{v}_{Fi} = v_{Fi}/[1 + \lambda_{ii} + \lambda_{ij}], \tag{20}$$

with

$$g(x) = \sum_{m=1}^{\infty} \frac{1}{(2m-1)^2}\frac{1}{|2m-1| + x}. \tag{21}$$

The function $g(x)$ has its maximum at $x=0$, i.e., for the clean limit, and drops like $1/x$ for large x (i.e., as $1/\pi t^+$ in the dirty limit). Equation (18) provides an algebraic expression for the dependence of the slope of the upper critical field on the electron-phonon parameters $\tilde{\lambda}_{ij}$, on the impurity scattering $\tilde{t}_{ii}^+$, and on the Fermi velocities $\tilde{v}_{Fi}$, all renormalized. First note that in the $\lambda_{\sigma\pi}=\lambda_{\pi\sigma}=0$ case (uncoupled bands) $A = \tilde{\lambda}_{\sigma\sigma} - \tilde{\lambda}_{\pi\pi}$ and the π-band drops out of Eq. (18), as it must. Further,

$$H_{c2}(T) = \frac{(1-t)\frac{6}{e}(\pi T_c)^2}{\tilde{v}_{F\sigma}^2 g_\sigma}, \tag{22}$$

which gives the known slope for any impurity content for the σ band on its own. In particular, for the clean limit $g_\sigma = 7\zeta(3)/4$ and in the dirty limit $g_\sigma = (T_c/\tilde{t}_{\sigma\sigma}^+)\pi^2/4$.

Next we note that the larger the value of $\tilde{v}_{Fi}$, the more the ith band is emphasized in the denominator of Eq. (18). On the other hand, the dirtier the band is, the more deemphasized it becomes. For the π band to influence the slope in a significant way, we need $\lambda_{\pi\sigma}$ and $\lambda_{\sigma\pi}$ to be finite, the σ band to be very dirty, and the π band clean. Furthermore, if the Fermi velocity for the σ band is small as compared with that of the π band, which is so for H in the ab plane, this further deemphasizes the role of the σ band in the slope. We note that the geometrical factor κ_i of Eq. (3) and Eq. (6), which we have set equal to 1 in this section, could also influence the relative role of π and σ bands. As a first application of Eq. (18) we show in Fig. 5 the results of RBCS for the slope $|T_c dH_{c2}(T)/dT|$ divided by T_c^2 in units of Tesla per Kelvin squared for a case with $\lambda_{\sigma\sigma}=1.0$, $\lambda_{\pi\pi}=0.5$. The continuous lines are for the three values of $\lambda_{\sigma\pi}=0.1, 0.3, 0.5$ as labeled in the figure. The horizontal scale is $\lambda_{\pi\sigma}$. Also shown for comparison are nine points which were obtained from full Eliashberg calculations. These results include the strong-coupling corrections not captured in RBCS. The solid squares are for $\lambda_{\sigma\pi}=0.1$, diamonds 0.3, and circles 0.5. For this set of parameters, not very different from those of MgB_2 as far as coupling strength is concerned, the corrections from retardation effects are of order 20% and both sets of results follow the same general trend. If we had contemplated larger values of T_c/ω_{ln} they could be larger. Here

$$\omega_{ln} \equiv \exp\left(\frac{2}{\lambda_{11}}\int_0^\infty \frac{\ln(\omega)\alpha_{11}^2 F(\omega)}{\omega} d\omega\right)$$

is the characteristic phonon energy that enters strong-coupling correction.[7,19]

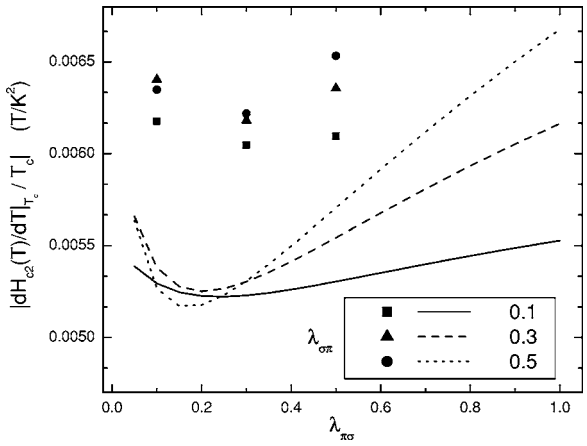

FIG. 5. The normalized slope of the upper critical field $H_{c2}(T)$ at T_c in the RBCS approximation as a function of $\lambda_{\pi\sigma}$. The continuous curves are for $\lambda_{\sigma\pi}=0.1$, 0.3, and 0.5. Here $\lambda_{\sigma\sigma}=1.0$ and $\lambda_{\pi\pi}=0.5$. The solid symbols give a comparison with full strong-coupling results.

V. IMPURITY DEPENDENCE OF *c*/*a*-*b* ANISOTROPY IN $H_{c2}(T)$

An important effect noted in MgB_2 is that the anisotropy in the ratio of the critical magnetic field in *ab* and *c* direction is very temperature-dependent.[8–11] Here we wish to understand how this anisotropy arises and how it depends on intraband impurity scattering, as well as how it will be modified by the interband scattering. While, as already stated, we do not attempt a fully realistic calculation for MgB_2, nevertheless for this study we start with electron-phonon parameters that are reasonably realistic for this case. While in Fig. 6 we have retained the stretched Pb spectrum for $\alpha_{ij}^2F(\omega)$, we have taken $\lambda_{\sigma\sigma}=1.012$, $\lambda_{\pi\pi}=0.448$, $\lambda_{\sigma\pi}=0.213$, and $\lambda_{\pi\sigma}=0.155$ and the $\mu^\star$'s are 0.21, 0.12, 0.09, and 0.09, respectively.[25] Of course in the two square-well model the $\mu_{ij}^\star$'s effectively get absorbed into the λ_{ij}'s. For simplicity, we have taken the *ab* Fermi velocities ratio $R\equiv v_{F\sigma}^2/v_{F\pi}^2=0.7$ but differing by a factor of $R=1/5$ in the *a*-*b* direction so as to get an anisotropy of order 5 in $\gamma_H(T)$ at $T=0$. In frame (a) of Fig. 6, we show γ_H versus reduced temperature $t=T/T_c$ for a clean σ band with varying values of $t_{\pi\pi}^+$, namely 0, 2, 5, 10, 20, 30, and 60 meV from bottom to top at T_c (the opposite order applies at $T=0$). We see that the amount of scattering in the π band can strongly influence the temperature dependence of γ_H. For the clean case, the anisotropy drops from 4.7 at $T=0$ to less than 3 at T_c. At intermediate values of $t_{\pi\pi}^+$, a comparatively flat curve is obtained and in the dirty case the anisotropy increases from about 3.3 at $T=0$ to nearly 4.8 at T_c. This complicated pattern of behavior has been noted in the experimental literature[11] and is also part of the earlier theoretical work of Gurevich[15] which is based on the Usadel equations, valid in the dirty limit, and no retardation effects are included.

In frame (b) of Fig. 6, we show additional results for a clean π band with $t_{\pi\pi}^+=0$ and $t_{\sigma\sigma}^+=0$, 2, 5, 30, and 60 meV, respectively, from top to bottom curves at $T=T_c$. Note that $\gamma_H(T)$ at $T=0$ is very slightly increased as $t_{\sigma\sigma}^+$ is increased.

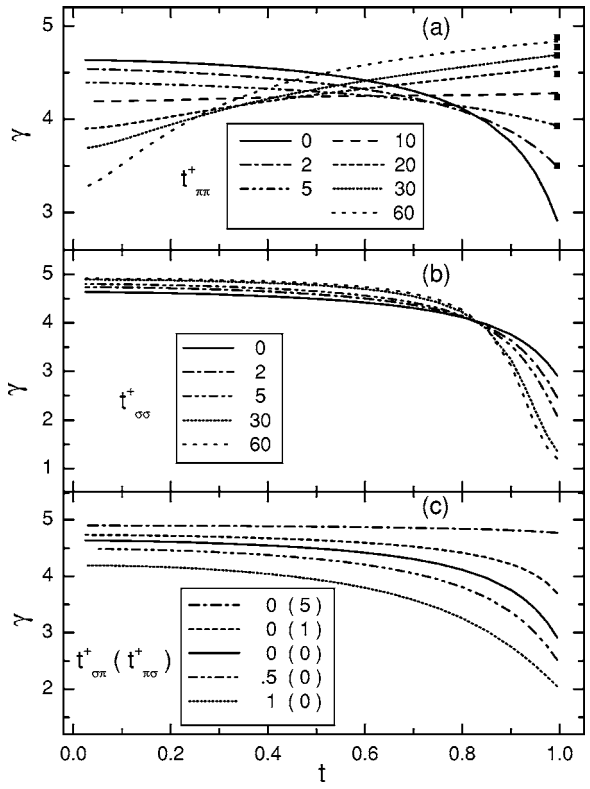

FIG. 6. Upper critical field anisotropy parameter as a function of reduced temperature $t=T/T_c$. Parameters are modeled for MgB_2 as described in the text. Frame (a) is for a clean σ band and various values of $t_{\pi\pi}^+$, namely 0, 2, 5, 10, 20, 30, and 60 meV as labeled. For frame (b), the π band is clean and $t_{\sigma\sigma}^+=0$, 2, 5, 30, and 60 meV as labeled. In frame (c), both σ and π bands are clean but interband scattering is considered. The middle curve (solid) is for $t_{\pi\sigma}^+=t_{\sigma\pi}^+=0$ and is for reference. The top curves are for $t_{\pi\sigma}^+=1$ and 5 meV while the bottom are for $t_{\sigma\pi}^+=0.54$ and 1.0 meV.

All curves show decreasing $\gamma_H(T)$ with increasing $t=T/T_c$ with overall anisotropy slightly increased as $t_{\sigma\sigma}^+$ increases. In frame (c) of this same figure, we present our results for the effect of interband impurity scattering on *ab*/*c* anisotropy. The middle curve (solid) applies to the clean case $t_{\pi\sigma}^+=t_{\sigma\pi}^+=0$ as well as $t_{\sigma\sigma}^+=t_{\pi\pi}^+=0$; it is included for comparison. For increasing value of $t_{\sigma\pi}^+=0.5$ and 1.0 meV we get the two lower curves, while the two upper ones are for $t_{\pi\sigma}^+=1.0$ and 5.0 meV. While $t_{\pi\sigma}^+$ increases γ_H at $T=0$, although not by much, it increases its value relatively more at T_c, making the overall curve flatter. The opposite applies to $t_{\sigma\pi}^+$. Also note that in all curves, T_c is reduced by both kinds of interband impurity scattering with $t_{\sigma\pi}^+$ the more effective variable (coupled bands). As previously noted, this gives the direct effect of the π band on the σ band and is more effective in reducing T_c. Of course in any realistic case the ratio $t_{\pi\sigma}^\dagger/t_{\sigma\pi}^\dagger$ is fixed by the ratio of the two densities of states $N_\sigma(0)$ and $N_\pi(0)$ so that these two parameters are not independent.

Next we consider the strong-coupling corrections for the anisotropy ratio $\gamma_H(T)$. At T_c in RBCS, we obtain from Eq. (18)

$$\gamma_H(T_c) = \frac{[\tilde{\lambda}_{\sigma\sigma} - \tilde{\lambda}_{\pi\pi} + A]g_\sigma + [\tilde{\lambda}_{\pi\pi} - \tilde{\lambda}_{\sigma\sigma} + A]g_\pi}{[\tilde{\lambda}_{\sigma\sigma} - \tilde{\lambda}_{\pi\pi} + A]g_\sigma R + [\tilde{\lambda}_{\pi\pi} - \tilde{\lambda}_{\sigma\sigma} + A]g_\pi}, \tag{23}$$

where we have assumed for simplicity that the *ab* and *c* Fermi velocities are all the same except for that of the σ band in the *ab* case, which is reduced by a factor of R. First, we consider several simple limits. For the decoupled case, $\gamma_H(T_c)=1/R$ and is independent of intraband impurities. For $\tilde{\lambda}_{\sigma\sigma}=\tilde{\lambda}_{\pi\pi}$, it is equal to $(1+g_\pi/g_\sigma)/(R+g_\pi/g_\sigma)$. For $g_\pi/g_\sigma \ll 1$ (dirty π band and clean σ band), we recover $1/R$ but in the opposite limit (clean π band and dirty σ band) it is equal to 1. To compare with the full strong-coupling results of Fig. 6, we need to use $R=1/5$ in Eq. (23) and use the λ's and $\mu^\star$'s previously introduced as representative of MgB_2. The solid squares of Fig. 6(a) at T near T_c are the results obtained from Eq. (23) with one modification. To conform with what is done in the Eliashberg program, we have inserted an extra factor of 0.7 in the numerator next to g_σ to account for the small difference in Fermi velocities in the *c* direction. Again it is seen that there are strong-coupling corrections but never larger than 10%, and for the case with $t^+_{\pi\pi}=60$ meV they become negligible.

Another case that gives very simple analytic expressions is the isotropic case for the electron-phonon interaction, namely $\lambda_{\pi\pi}=\lambda_{\sigma\sigma}=\lambda_{\sigma\pi}=\lambda_{\pi\sigma}=\lambda/2$. In this instance, the two energy gaps will be the same. This does not mean, however, that $\gamma_H(T)$ will not show any temperature dependence. Fermi velocity anisotropy encoded in Eqs. (1) and (2) remains, as does the possibility of differences in the intraband scattering rate. Thus even for $t^+_{\sigma\pi}=t^+_{\pi\sigma}=0$ these equations do not reduce to the one-band case. Rather we obtain

$$\tilde{\Delta}(n) = \pi T \sum_m \lambda(m-n)\frac{1}{2}\left[\frac{1}{\chi_\sigma^{-1}(|\tilde{\omega}_{m\sigma}|) - \pi t^+_{\sigma\sigma}} + \frac{1}{\chi_\pi^{-1}(|\tilde{\omega}_{m\pi}|) - \pi t^+_{\pi\pi}}\right]. \tag{24}$$

Reduction of Eq. (24) in the square-well model, and taking the limit of zero temperature, gives for the clean-clean limit

$$eH_{c2}(0) = \frac{[(1+\lambda)\pi T_c]^2 e^{-\gamma+2}}{2\sqrt{R}v_F^2}, \tag{25}$$

while for the dirty-dirty limit

$$eH_{c2}(0) = 3\pi e^{-\gamma}\frac{(\pi T_c)(1+\lambda)}{\sqrt{R}v_F^2}\sqrt{t^+_{\pi\pi}t^+_{\sigma\sigma}}, \tag{26}$$

and for the clean-dirty limit (i and j, respectively)

$$eH_{c2}(0) = \frac{2}{\tilde{v}_{Fi}^{2/3}\tilde{v}_{Fj}^{4/3}}\left(\frac{\pi T_c}{2}\right)^{4/3} e^{-\gamma+2/3}(3\pi\tilde{t}^+_j)^{2/3}, \tag{27}$$

where γ is Euler's constant and the tilde's mean normalization by a factor of $(1+\lambda)$. The above relationships combined with Eq. (18) for the slope evaluated in the isotropic gap limit give, for the clean-clean case,

$$h_{c2}(0) = 0.727\frac{R+1}{2\sqrt{R}},$$

$$\gamma_H(0) = \frac{1}{\sqrt{R}},$$

$$\gamma_H(T_c) = \frac{2}{1+R}; \tag{28}$$

for the dirty-dirty case,

$$h_{c2}(0) = \frac{0.69}{2\sqrt{R}}\left[R\sqrt{\frac{t^+_{\pi\pi}}{t^+_{\sigma\sigma}}} + \sqrt{\frac{t^+_{\sigma\sigma}}{t^+_{\pi\pi}}}\right],$$

$$\gamma_H(0) = \frac{1}{\sqrt{R}},$$

$$\gamma_H(T_c) = \frac{t^+_{\pi\pi} + t^+_{\sigma\sigma}}{Rt^+_{\pi\pi} + t^+_{\sigma\sigma}}; \tag{29}$$

for the σ-clean π-dirty case,

$$h_{c2}(0) = 0.316\frac{1}{R^{1/3}}[(1+\lambda)T_c]^2\left(\frac{t^+_{\pi\pi}}{(1+\lambda)T_c}\right)^{2/3} \times\left[R + 1.17\frac{T_c(1+\lambda)}{t^+_{\pi\pi}}\right],$$

$$\gamma_H(0) = \frac{1}{R^{2/3}},$$

$$\gamma_H(T_c) = \frac{1}{R}; \tag{30}$$

and for σ-dirty and π-clean,

$$h_{c2}(0) = 0.316\frac{1}{R^{2/3}}[(1+\lambda)T_c]^2\left(\frac{t^+_{\sigma\sigma}}{(1+\lambda)T_c}\right)^{2/3} \times\left[1 + 1.17R\frac{T_c(1+\lambda)}{t^+_{\sigma\sigma}}\right],$$

$$\gamma_H(0) = \frac{1}{R^{1/3}},$$

$$\gamma_H(T_c) = 1. \tag{31}$$

These simple formulas, while derived for the case of an isotropic gap, are nevertheless very useful and in a sense represent the other extreme, opposite to the limit of two completely decoupled systems. Here the off-diagonal matrix elements for the electron-phonon interaction are equal to the diagonal ones. In the clean-clean case, we see that $H_{c2}(0)$ increases as $1/\sqrt{R}$ for $R<1$ as does $h_{c2}(0)$ and that $\gamma_H(0)$ decreases with increasing temperature as shown in Fig. 6. To compare more specifically with the results given in frame (b) of Fig. 4, we can take $R=0.1$ in Eq. (28). We find $h_{c2}(0)$

$=1.26$, which shows that Fermi velocity anisotropy plays a large role in enhancing the value of $h_{c2}(0)$ as does the anisotropy in the λ_{ij}'s. This value also conforms to the trend noted previously, namely that the value $h_{c2}(0)$ is lower for $\lambda_{\pi\sigma}=\lambda_{\sigma\pi}=0.4$ than for 0.3. Further, we get $\gamma_H(0)=3.2$ and $\gamma_H(T_c)=0.8$ from Eq. (28) for $R=0.1$, which agrees well with the trend seen in frame (c) of Fig. 4. For the dirty-dirty case, $H_{c2}(0)$ of Eq. (26) increases with decreasing R (as $1/\sqrt{R}$) but also increases with increasing $t^+_{\pi\pi}$ and $t^+_{\sigma\sigma}$ as the square root of each. The normalized $h_{c2}(0)$ of Eq. (29) has a somewhat more complex behavior but is always $\geqslant 0.69$ (the one-band value). We note that γ_H at T_c is above its $T=0$ value for $R<1$ if the σ band is the cleanest of the two, and is below and near 1 if the π band is cleanest. In between these two cases, its value at T_c can fall close to its $T=0$ value. Thus this simple case exhibits the same three possible behaviors noted in Fig. 6. Finally for the clean-dirty case, γ_H goes up with increasing temperature [see Eq. (30)] and in the dirty-clean case it goes down [see Eq. (31)] as expected.

We have already noted in Fig. 3 the upward curvature of the $H_{c2}(t)$ near T_c. For the isotropic energy gap case, we can derive an analytic expression for this curvature,

$$eH_{c2}(t)=\frac{(\pi T_c)^2}{\tilde{v}^2_{F\sigma}+\tilde{v}^2_{F\pi}}\left[5.7(1-t)+2.86\left(6.52\frac{R^2+1}{(R+1)^2}-3\right)(1-t)^2\right]. \quad (32)$$

For $R=1$ equal Fermi velocities in σ and π bands, this reduces to the one-band form with the ratio of the coefficient of the quadratic to that of the linear term equal to 0.13. For the case $R=0$, as an extreme example, it is instead 1.75, an order of magnitude larger. The coefficient of the quadratic term is now larger than that for the linear term in $(1-t)$. We see that a smaller Fermi velocity in the σ band leads to the upward curvature seen in Fig. 3. Of course we also saw in this figure that the amount depends not only on R but also on the anisotropy in the λ_{ij}'s; the latter is not part of the simpler formula given by Eq. (32), which is restricted to the isotropic gap case. As we have already emphasized, curvature near T_c is often seen in experiment for H oriented in the ab plane.

Examination of the general structure of the equations for $H_{c2}(T)$ shows that increasing the impurity content of a subband plays a similar role to decreasing its Fermi velocity. This has been noted with reference to Eq. (18) for the slope of $H_{c2}(T)$ at T_c in RBCS, but holds generally. Thus, we would expect to also see an upward curvature in $H_{c2}(T)$ near T_c for the c direction where both Fermi velocities are assumed to have the same value but the σ band is dirty while the π band is clean. This is seen in Fig. 7, where we have used parameters that roughly model MgB_2. For the solid curve, both bands are assumed clean while for the dotted curve $t^+_{\sigma\sigma}=60$ meV and for the dashed curve $t^+_{\pi\pi}=60$ meV. These curves have exactly the same general behavior as we found in frame (c) of Fig. 3, where the Fermi velocities were taken different for the π and σ band while both were assumed clean. Note that for the curves in Fig. 7, the anisotropy in the λ_{ij}'s is fully included, in contrast to our earlier

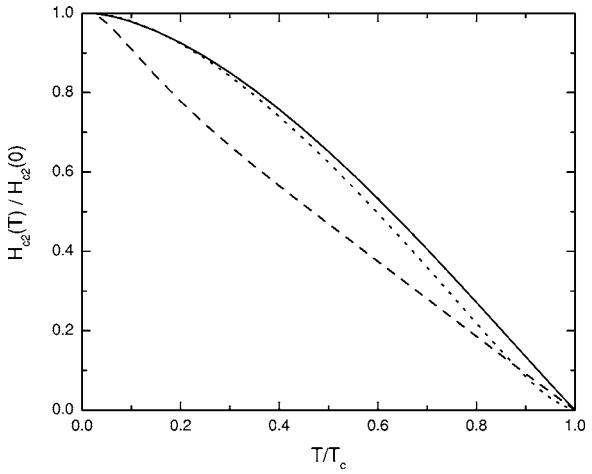

FIG. 7. The normalized upper critical field $H_{c2}(t)$ vs reduced temperature $t=T/T_c$ for $H\|c$ using model parameters (as in Fig. 6) for MgB_2. The solid curve applies when both bands are clean, the dotted when $t^+_{\sigma\sigma}=60$ meV (clean π band and dirty σ band), and the dashed when $t^+_{\pi\pi}=60$ meV (dirty π band and clean σ band).

simple analytic results [based on Eq. (24)], for which it was assumed that all λ_{ij} had the same value (i.e., no gap anisotropy). In this limit, as an example, the thermodynamics would reduce to the one-band case. However, this does not apply to H_{c2}, which is also dependent on Fermi surface anisotropy and possible differences in intraband scattering in the π and σ bands. The quasilinear behavior seen in the dashed curve near T_c is characteristic of two bands with π dirty and σ clean, while the upward curvature near T_c is characteristic of dirty σ with clean π.

We have derived an analytic expression for the curvature in $H_{c2}(T)$ near T_c for the general case in RBCS. We find

$$\left.\frac{T_c^2H''_{c2}(T)}{T_cH'_{c2}(T)}\right|_{T_c}=-\left[1-\frac{2\Lambda}{a}\right]+\frac{2}{b}[(G_{1\pi}+G_{1\sigma})2\Lambda+T_c(G'_{1\sigma}+G'_{1\pi})a+(G'_{1\sigma}-G'_{1\pi})T_c(\tilde{\lambda}_{\sigma\sigma}-\tilde{\lambda}_{\pi\pi})]-\frac{4a}{b^2}[(\tilde{\lambda}_{\sigma\sigma}-\tilde{\lambda}_{\pi\pi})(G_{2\sigma}-G_{2\pi})+(G_{2\sigma}+G_{2\pi})a-2\Lambda G_{1\sigma}G_{1\pi}], \quad (33)$$

with

$$\Lambda=\tilde{\lambda}_{\sigma\sigma}\tilde{\lambda}_{\pi\pi}-\tilde{\lambda}_{\pi\sigma}\tilde{\lambda}_{\sigma\pi},$$

$$a=\sqrt{(\tilde{\lambda}_{\sigma\sigma}-\tilde{\lambda}_{\pi\pi})^2+4\tilde{\lambda}_{\sigma\pi}\tilde{\lambda}_{\pi\sigma}},$$

$$b=(\tilde{\lambda}_{\sigma\sigma}-\tilde{\lambda}_{\pi\pi})(G_{1\pi}-G_{1\sigma})-(G_{1\sigma}+G_{1\pi})a. \quad (34)$$

Here

$$G_{1j}=-\frac{e}{6}v^2_{Fj}\frac{\pi T_c}{1+\lambda_j}\sum_m\frac{1}{\omega_m^2|\tilde{\omega}_{mj}|},$$

$$G_{2j}=\frac{e}{4}v^4_{Fj}\frac{\pi T_c}{1+\lambda_j}\sum_m\left[\frac{13}{45\omega_m^2|\tilde{\omega}_{mj}|^3}+\frac{1}{9}\frac{1}{(1+\lambda_j)|\omega_m|^3\tilde{\omega}^2_{mj}}\right],$$

$$G'_{1j} = -\frac{1}{T_c}(G_{1j} + G_{3j}), \tag{35}$$

with G_{3j} the same as G_{1j} but with a single power of ω_m and two powers of $\tilde{\omega}_{mj}$ in the sum over Matsubara frequencies and no $(1+\lambda_j)$ factor.

In the clean limit,

$$G_{ij} = -[7\zeta(3)/8](e/3)\tilde{v}_{Fj}^2/(\pi T_c)^2,$$

$$G_{3j} = G_{1j},$$

$$G_{2j} = [4/5](e^2/4)\tilde{v}_{Fj}^4/(\pi T_c)^4,$$

where $\zeta(3)$ is the Riemann zeta function. Equation (33) greatly simplifies in this limit and we get

$$\left.\frac{T_c^2 H''_{c2}(T)}{T_c H'_{c2}(T)}\right|_{T_c} = -\left[1 - \frac{2\Lambda}{a}\right] + \frac{4}{b}[(\Lambda - a)(R+1) - (R-1) \times (\tilde{\lambda}_{\sigma\sigma} - \tilde{\lambda}_{\pi\pi})] - \frac{4a}{\bar{b}^2}[1.63\{(\tilde{\lambda}_{\sigma\sigma} - \tilde{\lambda}_{\pi\pi}) \times (R^2-1) + a(R^2+1)\} - 2\Lambda R], \tag{36}$$

with

$$\bar{b} = (\tilde{\lambda}_{\sigma\sigma} - \tilde{\lambda}_{\pi\pi})(1-R) - a(1+R). \tag{37}$$

Equation (36) for the normalized curvature at $T=T_c$ involves only the anisotropy parameters λ_{ij}'s and $R \equiv \tilde{v}_{F\sigma}^2/\tilde{v}_{F\pi}^2$, the ratio of the two Fermi velocities. As an example for $\lambda_{\sigma\sigma}=1$, $\lambda_{\pi\pi}=0.5$, and $\lambda_{\pi\sigma}=\lambda_{\sigma\pi}=0.2$, expression (36) equals -17 for $R=0$ while for the isotropic gap case it is only ~ -3.5. Our strong-coupling programs give -21.7 and -3.3. Gap anisotropy has increased the curvature by a large amount. By contrast, for $R=1$, the isotropic and anisotropic gap cases give almost the same value of ~ -0.26. This occurs because in that case the terms proportional to $(\tilde{\lambda}_{\sigma\sigma} - \tilde{\lambda}_{\pi\pi})$ and Λ in Eqs. (36) and (37) drop out and no anisotropy parameter remains.

In Fig. 8, we give results for the impurity dependence of the normalized curvature $\delta \equiv |[T_c^2 (d^2H_c/dT^2)|_{T_c}]/[T_c (dH_c/dT)|_{T_c}]|$ of H_{c2} at T_c. The parameters employed are those previously introduced to model the specific case of MgB_2 (see Ref. 25) as in Figs. 6 and 7. Frame (a) gives its dependence as $t^+_{\sigma\sigma}$ or $t^+_{\pi\pi}$ is varied. The solid and dash-dotted lines are for varying $t^+_{\sigma\sigma}$ while dashed and dotted lines are for varying $t^+_{\pi\pi}$, with $R=0.1$ and $R=0.7$, respectively. Intraband impurity scattering for the σ band leads to a large enhancement of the normalized curvature as well as of the corresponding value of $h_{c2}(0)$, which is shown in frame (b). Also the smaller value of R gives higher values for both curvature and $h_{c2}(0)$. This behavior agrees qualitatively with our simple formula [i.e., Eq. (31)], which, of course, applies only to the special case of no gap anisotropy and to the dirty limit for the σ band. In contrast to the above, when $t^+_{\pi\pi}$ is increased, the normalized curvature initially rapidly drops from its value in the clean case to much smaller values (nearly zero) and remains small even at the largest values of $t^+_{\pi\pi}$ considered. A similar pattern is seen for the case of $h_{c2}(0)$ [frame (b)], which remains near 1 in the figure with a slight upward trend at large values of $t^+_{\pi\pi}$. This behavior is in qualitative agreement with Eq. (30).

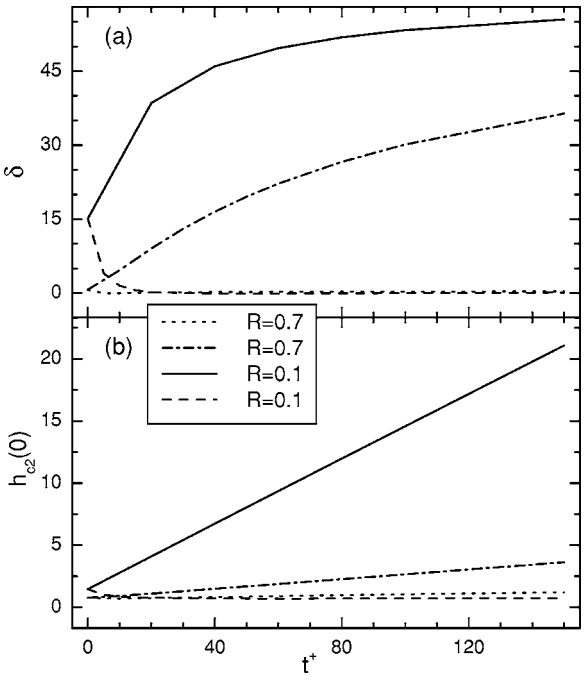

FIG. 8. Frame (a): the normalized curvature for $H_{c2}(T)$ at T_c namely $\delta \equiv |[T_c^2 (d^2H_c/dT^2)|_{T_c}]/[T_c (dH_c/dT)|_{T_c}]|$ as a function of intraband impurity scattering t^+_{ii}. Solid and dash-dotted lines are for $t^+_{\sigma\sigma}$, while dashed and dotted lines are for $(t^+_{\pi\pi})$. Frame (b): results for $h_{c2}(0)$ in the same format. Parameters are modeled for MgB_2.

VI. SUMMARY AND CONCLUSIONS

We have used a generalization of the original microscopic equations of Werthamer, Helfand, and Hohenberg for $H_{c2}(T)$ to discuss its dependence on the electron-phonon spectral densities and on their anisotropy, as well as on different values of the Fermi velocities in a two-band model. The generalized equations include retardation effects (strong-coupling corrections) and are valid for arbitrary value of intra as well as interband impurity scattering. In the case of independent bands, which result when there is no off-diagonal electron-phonon interactions and no interband elastic scattering, we find that the π band (lower gap value) can enter at lower temperature provided it is sufficiently dirty or has a very small Fermi velocity as compared with the σ band (higher gap value), while at the same time it is the σ band on its own which determines the value of T_c. In such a case, the value of the zero-temperature critical field normalized to its slope at T_c, $h_{c2}(0)$, can be larger than its canonical one-band value of 0.727 (clean) and 0.69 (dirty). Further, the temperature dependence of $H_{c2}(T)$ shows a crossover behavior at the specific value of T where the second band enters. When the off-diagonal electron-phonon interaction is switched on, the region of the crossover point rapidly smears even for small values of the corresponding electron-phonon mass renormalization parameters $\lambda_{\sigma\pi}=\lambda_{\pi\sigma}\sim 0.05$ but the normalized value

of $h_{c2}(0)$ does not change much, keeping its somewhat enhanced value. This is characteristic of two-band superconductivity in this regime. Another characteristic is that the curves for $H_{c2}(T)$ naturally take on a quasilinear T dependence over a relatively large range of temperature, as noted in experiments on MgB_2.

We have considered the effect of interband impurity scattering $t^+_{\sigma\pi}$ and $t^+_{\pi\sigma}$ in the regime of no interband electron-phonon coupling. The signature of the crossover remains in all cases until the entire direct contribution of the π band simply disappears. We find that $t^+_{\sigma\pi}$ and $t^+_{\pi\sigma}$ have quite different effects. The parameter $t^+_{\sigma\pi}$ gives the effect of the π band on the σ band and is highly effective at reducing the value of T_c as well as the contribution of the σ band to $H_{c2}(T)$ leaving that from the π band relatively unaltered and moving the crossover to a higher value of T. By contrast, $t^+_{\pi\sigma}$ does not change T_c and the contribution of the σ band to $H_{c2}(T)$, but it suppresses the magnitude of the direct contribution of the π band to $H_{c2}(T)$. The crossover temperature is reduced but does not smear. Eventually the second contribution of the π band completely disappears.

It has been noticed in MgB_2 that the anisotropy ratio $\gamma_H(T)$ shows considerable temperature dependence and that different samples show different behaviors. Using electron-phonon parameters in the range realistic for the case of MgB_2, we find a complex pattern of variation for the T dependence of $\gamma_H(T)$ depending on in-band impurity scattering. For a clean σ band and various values of $t^+_{\pi\pi}$, we find three regimes. For small values of $t^+_{\pi\pi}$, γ_H decreases with increasing T; at intermediate values, it stays reasonably flat; and at large values, it increases with T. Also, for a fixed value of the Fermi velocity anisotropy, the value of $\gamma_H(0)$ decreases with increasing $t^+_{\pi\pi}$ while its value at $T=T_c$ increases. Impurities play a key role in the T behavior of the anisotropy parameter $\gamma_H(T)$ and also on its magnitude. However, $\gamma_H(T)$ is also affected by the anisotropy in the electron-phonon interaction, particularly by $\lambda_{\sigma\pi}$ and $\lambda_{\pi\sigma}$ and, of course, by the band Fermi velocities. We have studied these independently. Increasing $\lambda_{\sigma\pi}=\lambda_{\pi\sigma}$ can decrease the anisotropy in the T dependence of $\gamma_H(T)$ while also decreasing its magnitude at $T=0$. The magnitude of $\gamma_H(0)$ strongly depends on Fermi velocity anisotropy in the σ band. Further interband impurity scattering $t^+_{\sigma\pi}$ ($t^+_{\pi\sigma}$) decreases (increases) its zero-temperature magnitude and increases (decreases) its T dependence.

We have applied a $\lambda^{\theta\theta}$ or two-square-well approximation to reduce our Eliashberg equations to a renormalized BCS form. These simpler equations have the important property that they allow for analytic results in several cases. The slope of the critical field at $T=T_c$ and its curvature can be obtained in a closed form for arbitrary intraband impurity content and other parameters. These are important because they allow one to see specifically how various normal-state parameters such as the electron-phonon $\tilde{\lambda}_{ij}$, the Fermi velocities $\tilde{v}_{Fi}$, etc., affect these quantities. Comparison of RBCS with full Eliashberg results also allows us to identify the so-called strong-coupling corrections which have their origin in the retardation effects. For the slope of H_{c2} at T_c and for the anisotropy parameter γ_H also at T_c, they are found to be of order 20% for parameters realistic to MgB_2. In other cases, they could be more significant. In our complete Eliashberg solutions, we found that $H_{c2}(T)$ near T_c acquires an upward curvature when the Fermi velocity in the σ band is much smaller than in the π band, as is the case in MgB_2 when the magnetic field H is oriented in the ab plane. Also, a similar curvature results for H along the c axis if the σ band is dirty and the π band is clean. Accompanying these large values of curvature are large values of $h_{c2}(0)$. Using our renormalized BCS results in the case when gap anisotropy is neglected (i.e., in the limit when all the electron-phonon λ_{ij}'s are equal), we derive analytic results for the curvature at T_c which confirm our numerical results. It is also clear from this analysis that increasing $t^+_{\sigma\sigma}$ while leaving $t^+_{\pi\pi}=0$ has a similar effect to that for a small value of $v_{F\sigma}$. We have shown analytically, in the clean limit, that anisotropy in the λ_{ij}'s when $v_{F\sigma}<v_{F\pi}$ can enhance the curvature even more. Further, in the dirty or clean limit for either or both bands, we derive very simple expressions for $H_{c2}(0)$, $h_{c2}(0)$, $\gamma_H(0)$, and $\gamma_H(T_c)$ valid in the isotropic gap case which show explicitly their dependence on intraband impurity scattering and on Fermi velocity anisotropy. While limited in their region of validity, they provide insight into the numerical results obtained in the more general case. Finally, we showed that intraband impurity scattering $t^+_{\sigma\sigma}$ can greatly increase the upward curvature at $T=T_c$ and the value of $h_{c2}(0)$. $t^+_{\pi\pi}$ rapidly reduces the curvature to a value close to zero and $h_{c2}(0)$ drops toward 1, followed by a modest increase at large values of $t^+_{\pi\pi}$.

ACKNOWLEDGMENTS

Research supported in part by the Natural Sciences and Engineering Council of Canada (NSERC), the Canadian Institute for Advanced Research (CIAR), and Al-Fateh University, Tripoli, Libya. We thank E. Nicol and A. Knigavko for their interest and critical comments.

APPENDIX A: GENERALIZATION TO TWO ANISOTROPIC BANDS

The s-wave one-band equation from Prohammer and Carbotte[23] for the inhomogeneous gap at $\mathbf{R}$ is given by

$$\phi(\mathbf{R},\omega_n) = T\sum_m \frac{1}{(2\pi)^3}\int d^3\mathbf{q}\,\alpha^2 D(\omega_n-\omega_m) \times \int d^3\mathbf{y}\int d^3\mathbf{z} e^{i\mathbf{q}\cdot(\mathbf{y}-\mathbf{z})} G_0(\mathbf{y};\omega_m) \times G_0^{\star}(\mathbf{y};\omega_m) e^{i\mathbf{z}\cdot\mathbf{\Pi}(\mathbf{R})}\phi(\mathbf{R};\omega_m), \tag{A1}$$

where

$$\mathbf{\Pi}(\mathbf{R}) = \frac{1}{i}\nabla_{\mathbf{R}} + ie\mathbf{A}(\mathbf{R}) \tag{A2}$$

and

$$G_0(\mathbf{y};\omega_m) = \frac{1}{(2\pi)^3}\int d^3\mathbf{k}\frac{e^{i\mathbf{k}\cdot\mathbf{y}}}{i\tilde{\omega}_m - \tilde{\epsilon}_k}. \tag{A3}$$

We now make the generalization to two bands and gaps,

$$\phi_i(\mathbf{R},\omega_{jn}) = T\sum_{mj}\frac{1}{(2\pi)^3}\int d^3\mathbf{q}_j\alpha^2 D_{ij}(\omega_{jn}-\omega_{jm}) \times \int d^3\mathbf{y}\int d^3\mathbf{z}e^{i\mathbf{q}_j\cdot(\mathbf{y}-\mathbf{z})}G_{0j}(\mathbf{y};\omega_{jm}) \times G^{\star}_{0j}(\mathbf{y};\omega_{jm})e^{i\mathbf{z}\cdot\mathbf{\Pi}(\mathbf{R})}\phi_j(\mathbf{R};\omega_{jm}). \quad \text{(A4)}$$

Using the same transformation (local) on each band by itself, we reach an equivalent formula to Eq. (17) in Prohammer and Carbotte,[23] viz.,

$$\phi_i(\mathbf{R}')\Delta_i(\omega_{in}) = \frac{T}{2}\sum_{mj}\int\frac{d^3\mathbf{k}'_j}{k'^2_j}\frac{e^{-2|\tilde{\omega}_{jm}|k'_j/v'_{Fj}}}{v'_{Fj}}e^{-i\,\mathrm{sgn}(\tilde{\omega}_{jm})\mathbf{k}'_j\cdot\mathbf{\Pi}'(\mathbf{R}')} \times\lambda_{ij}(n-m)\phi_j(\mathbf{R}')\Delta_j(\omega_{jm}). \quad \text{(A5)}$$

With also the same kind of local relations for each band and gap, we get the eigenfunction appropriate to the largest field H value as

$$\phi_j(\mathbf{R}) = \exp\left(-\frac{2\alpha}{1+\kappa_j}(R_y^2+\kappa_j R_x^2)\right), \quad \text{(A6)}$$

where $\alpha=eH/2$. Substituting these two solutions into Eq. (A4), we get

$$\phi_i(\mathbf{R})\Delta_i(\omega_{in}) = \frac{T}{2}\sum_{mj}\lambda_{ij}(n-m)\int\frac{d^3\mathbf{k}'_j}{k'^2_j}\frac{e^{-2|\tilde{\omega}_{jm}|k'_j/v'_{Fj}}}{v'_{Fj}} \times e^{-(k''^2_{xj}+k''^2_{yj})\kappa_j\alpha}\Delta_j(\omega_{jm})\phi_j(\mathbf{R}). \quad \text{(A7)}$$

Now we integrate over R_x and R_y to obtain

$$\pi\frac{1+\kappa_i}{2\alpha}\frac{1}{\sqrt{\kappa_i}}\Delta_i(\omega_{in}) = \frac{T}{2}\sum_{mj}\lambda_{ij}(n-m)\int\frac{d^3\mathbf{k}'_j}{k'^2_j}\frac{e^{-2|\tilde{\omega}_{jm}|k'_j/v'_{Fj}}}{v'_{Fj}} \times e^{-(k''^2_{xj}+k''^2_{yj})\kappa_j\alpha}\Delta_j(\omega_{jm})\pi\frac{1+\kappa_j}{2\alpha}\frac{1}{\sqrt{\kappa_j}}, \quad \text{(A8)}$$

and now we perform the Fourier transform to get

$$\frac{1+\kappa_i}{\sqrt{\kappa_i}}\Delta_i(n) = \pi T\sum_{mj}\lambda_{ij}(n-m)\chi_j(m)\Delta_j(m)\frac{1+\kappa_j}{\sqrt{\kappa_j}}. \quad \text{(A9)}$$

We renormalize the gaps by

$$\tilde{\Delta}_{in} = \Delta_{in}\frac{1+\kappa_i}{\sqrt{\kappa_i}}, \quad \text{(A10)}$$

so we get

$$\tilde{\Delta}_{in} = \pi T\sum_{mj}\lambda_{ij}(n-m)\chi_j(m)\tilde{\Delta}_{jm}, \quad \text{(A11)}$$

with

$$\chi_i(n) = \frac{2}{\sqrt{\alpha_i}}\int_0^{\infty}dq e^{-q^2}\tan^{-1}(\beta_{in}q),$$

$$\beta_{in} = \frac{\sqrt{\alpha_i}}{|\tilde{\omega}_{in}|}, \quad \alpha_i = \alpha v'^2_{Fi}\kappa_i, \quad \alpha = eH/2, \quad \text{(A12)}$$

where v'_{Fi} is the isotropic Fermi velocity of each band after transformation using the dispersion

$$\epsilon_{ik} = \frac{1}{2m_i}(k'^2_x+k'^2_y+k'^2_z). \quad \text{(A13)}$$

[1] J. Nagamatsu, N. Nakagawa, T. Muranaka, X. Zenitani, and J. Akimitsu, Nature (London) **410**, 63 (2001).
[2] M. Iavarone, G. Karapetrov, A. E. Koshelev, W. K. Kwok, G. W. Crabtree, D. G. Hinks, W. N. Kang, E.-M. Choi, H. J. Kim, H.-J. Kim, and S.-I. Lee, Phys. Rev. Lett. **89**, 187002 (2002).
[3] R. S. Gonnelli, D. Daghero, G. A. Ummarino, V. A. Stepanov, J. Jun, S. M. Kazakov, and J. Karpinski, Phys. Rev. Lett. **89**, 247004 (2002).
[4] A. Y. Liu, I. I. Mazin, and J. Kortus, Phys. Rev. Lett. **87**, 087005 (2001).
[5] H. J. Choi, D. Roundy, H. Sun, M. L. Cohen, and S. G. Louie, Nature (London) **418**, 758 (2002).
[6] A. Brinkman, A. A. Golubov, H. Rogalla, O. V. Dolgov, J. Kortus, X. Kong, O. Jepsen, and O. K. Andersen, Phys. Rev. B **65**, 180517(R) (2002).
[7] E. J. Nicol and J. P. Carbotte, Phys. Rev. B **71**, 054501 (2005).
[8] M. Angst, R. Puzniak, A. Wisniewski, J. Jun, S. M. Kazakov, J. Karpinski, J. Roos, and H. Keller, Phys. Rev. Lett. **88**, 167004 (2002).
[9] Yu. Eltsev, S. Lee, K. Nakao, N. Chikumoto, S. Tajima, N. Koshizuka, and M. Murakami, Phys. Rev. B **65**, 140501(R) (2003).
[10] L. Lyard, P. Samuely, P. Szabo, T. Klein, C. Marcenat, L. Paulius, K. H. P. Kim, C. U. Jung, H.-S. Lee, B. Kang, S. Choi, S.-I. Lee, J. Marcus, S. Blanchard, A. G. M. Jansen, U. Welp, G. Karapetrov, and W. K. Kwok, Phys. Rev. B **66**, 180502(R) (2002).
[11] V. Ferrando, C. Tarantini, B. Bellingeri, P. Manfrinetti, I. Pallecchi, D. Marre, M. Putti, O. Plantevin, R. Felici, and G. Ferdeglini, Supercond. Sci. Technol. **17**, 1434 (2004).
[12] A. A. Golubov and A. E. Koshelev, Phys. Rev. B **68**, 104503 (2003).
[13] A. E. Koshelev and A. A. Golubov, Phys. Rev. Lett. **92**, 107008 (2004).
[14] V. G. Kogan and S. L. Bud'ko, Physica C **385**, 131 (2003).
[15] A. Gurevich, Phys. Rev. B **67**, 184515 (2003).
[16] T. Dahm and N. Schopohl, Phys. Rev. Lett. **91**, 017001 (2003).
[17] C. T. Rieck, K. Scharnberg, and N. Schopohl, J. Low Temp. Phys. **84**, 381 (1991).
[18] N. R. Werthamer, E. Helfand, and P. C. Hohenberg, Phys. Rev. **147**, 295 (1966).
[19] J. P. Carbotte, Rev. Mod. Phys. **62**, 1027 (1990).
[20] M. Schossmann and E. Schachinger, Phys. Rev. B **33**, 6123 (1986).

[21] M. Prohammer and E. Schachinger, Phys. Rev. B **36**, 8353 (1987).
[22] S. V. Shulga, S. L. Drechsler, G. Fuchs, K. H. Müller, K. Winzer, M. Heinecke, and K. Krug, Phys. Rev. Lett. **80**, 1730 (1998).
[23] M. Prohammer and J. P. Carbotte, Phys. Rev. B **42**, 2032 (1990).
[24] P. Entel and M. Peter, J. Low Temp. Phys. **22**, 613 (1976).
[25] A. A. Golubov, J. Kortus, O. V. Dolgov, O. Jepsen, Y. Kong, O. K. Andersen, B. J. Gibson, K. Ahn, and R. K. Kremer, J. Phys.: Condens. Matter **14**, 1353 (2002).
[26] B. Mitrovic, Eur. Phys. J. B **38**, 451 (2004).
[27] S. V. Shulga, S. L. Drechsler, H. Eschrig, H. Rosner, and W. Pickett, e-print cond-mat/0103154.
[28] T. Dahm, S. Graser, and N. Schopohl, Physica C **408–410**, 336 (2004).
[29] M. Putti, V. Braccini, C. Ferdeghini, I. Pallecchi, A. S. Siri, F. Gatti, P. Manfrinetti, and A. Palenzona, Phys. Rev. B **70**, 052509 (2004).
[30] M. Putti, C. Ferdeghini, M. Monni, I. Pallecchi, C. Tarantini, P. Manfrinetti, A. Palenzona, D. Daghero, R. S. Gonnelli, and V. A. Stepanov, Phys. Rev. B **71**, 144505 (2005).
[31] V. Braccini, A. Gurevich, J. E. Giencke, M. C. Jewell, C. B. Eom, D. C. Larbalestier, A. Pogrebnyakov, Y. Cui, B. T. Liu, Y. F. Hu, J. M. Redwing, Q. Li, X. X. Xi, R. K. Singh, R. Gandikota, J. Kim, B. Wilkens, N. Newman, J. Rowell, B. Moeckly, V. Ferrando, C. Tarantini, D. Marre, M. Putti, C. Ferdeghini, R. Vaglio, and E. Haanappel, Phys. Rev. B **71**, 012504 (2005).
[32] B. Kang, H.-J. Kim, M.-S. Park, K.-H. Kim, and S.-I. Lee, Phys. Rev. B **69**, 144514 (2004).
[33] V. Ferrando, P. Manfrinetti, D. Marre, M. Putti, I. Sheikin, C. Tarantini, and C. Ferdeghini, Phys. Rev. B **68**, 094517 (2003).